JOURNAL OF PETROLEUM GEOMECHANICS
(JPG)

Original article

Investigating the effects of conductive-convective heat transfer on hydraulic fracturing via a fully coupled THM analysis using an enriched EFG method

Mohammad Ali Iranmanesh[1*], Ali Pak[2]

1- Assistant Professor, Department of Civil Engineering, K. N. Toosi University of Technolog, Tehran, Iran
2- Professor, Department of Civil Engineering, Sharif University of Technolog, Tehran, Iran

Received: 2 May 2022 ; Accepted: 19 July 2022

DOI: 10.22107/jpg.2022.363144.1180

Keywords

**Hydraulic Fracturing,
Element Free Galerkin,
Extrinsic Enrichment,
Thermo-Hydro-Mechanical Analysis,
Cohesive Crack Model**

Abstract

In this study, an eniched element free Galerkin framework is developed to investigate the effects of conductive-convective heat transfer on hydraulic fracturing. Weak and strong discontinuities are introduced in field variables using the enrichment strategy. The cohesive crack model is used in this study to simulate the process of initiation and propagation of fractures in saturated deformable porous media. The complicated process of hydraulic fracturing with thermal effects is simulated considering multiple components including fluid flow within the fracture, fluid flow through the host medium, fluid leak-off from the fracture into the surrounding porous rock, heat transfer within the fracture medium, heat transfer through the host porous rock, the heat exchange between the crack medium and the surrounding media, deformation of porous rock due to the hydraulic and thermal loading and crack propagation. To create the discrete equation system, Galerkin technique is applied, and the essential boundary conditions are imposed via penalty method. Then, the resultant constrained integral equations are discretized in space using EFG shape functions. For temporal discretization, a fully implicit scheme is employed. The final set of algebraic equations that form a non-linear equation system are solved using the iterative Newton-Raphson procedure. Numerical simulation results show the accuracy of the formulation as well as the performance of the program in coupling the heat transfer equation inside the crack with other governing equations.

1. Introduction

Enhanced oil recovery (EOR) techniques, particularly hydraulic fracturing, have become important topics in the thermo-hydro-mechanical analysis of multi-phase porous media. Hydraulic fracturing can be defined as a phenomenon in which a crack appears and propagates in the ground due to the hydraulic load applied by a viscous fluid. The process of creating hydraulic fractures in underground layers has been widely used in various engineering applications over the past few decades. It is a major technique to stimulate damaged oil/gas wells and unconventional with very low reservoirs permeability. It provides large cracks with high hydraulic conductivity to enhance the oil and gas flow rate from hydrocarbon reservoirs of poor permeability towards the wellbores. Many experimental, analytical, and numerical studies have been devoted to the hydraulic fracturing in recent years [1]–[10]. The thermal effects on different aspects of hydraulic fracturing are being studied by a number of researchers. For instance Tiankui et al. [11] conducted a numerical analysis of hydraulic fracturing of hot dry rocks. Liu et al. [12] investigated the effects of temperature field on elasto-plastic hydraulic fracture propagation in deep reservoirs. Luo et al. [13] analysed the THM behavior of hydraulic fracturing in naturally fractured formation. Zhou et al. [14] conducted

* Department of Civil Engineering, K. N. Toosi University of Technology, Valiasr Street, Mirdamad Intersection, Tehran, Iran. Email: Iranmanesh@kntu.ac.ir

numerical simulation of hydraulic fracturing in enhanced geothermal systems. Yan et al. [15] presented a FDEM-based 2D coupled THM model for rock fracturing. The thermal cooling effects to improve hydraulic fracturing efficiency and hydrocarbon production in shales is investigated by Enayatpour et al. [16]. Some other researchers investigated the effects of cooling or heating on fractured and/or fracturing porous media [17]–[19].

In this study the three-dimensional fluid flow in saturated deformable porous media is considered under conductive and convective heat transfer using the element-free Galerkin (EFG) method. Application of conventional finite element method [20], [21], control volume based finite element method [22], [23] and other numerical frameworks such as mesh-free methods [24]–[27] in simulation of saturated/unsaturated deformable porous media has already been demonstrated by a number of researchers. The proposed formulation considers the solid phase displacement in three directions, fluid phase pressure, and temperature as the main variables. The solid phase is assumed to be in temperature equilibrium with liquid phase; i.e., the solid phase and fluid phase have the same temperature at each time, and there was no temperature difference between phases [28].

The governing partial differential equations include the linear momentum balance equation of the system, the continuity equation of fluid phase, and the heat transfer equation. The weak forms of the governing equations are developed by discretization in space using the EFG method and are discretized in time domain using the finite difference method and a fully implicit scheme. Since the moving least squares (MLS) shape functions in EFG lack the Kronecker delta, the boundary conditions are imposed using the penalty method [29]. Application of EFG for Thermo-Hydro-Mechanical simulations of saturated and unsaturated porous media in continuous and discontinuous deformable porous media has already been demonstrated by Iranmanesh et al. [24] and Iranmanesh and Pak [30]. The fully coupled algebraic equation system was solved via the Newton-Raphson method. This study assumed elastic geomechanical behavior for rocks. To model weak and strong discontinuities in the displacement fields, pore fluid pressure, and temperature, external enrichment was implemented. So, fracture propagation, fluid flow through cracks, flow exchange between cracks and medium, heat transfer inside the fracture and hydraulic fracture propagation could be modeled. Since the fracture process zone length in the crack tip is not negligible compared to the crack length in semi-brittle materials such as rocks, the cohesive crack model was employed to describe the nonlinear fracture processes at the crack tip [31].

The host reservoir rock was assumed to be a saturated porous media, and the interactions between all the physical phenomena governung the propagation of hydraulic fracturing were incorporated into the model. These physical phenomena include the flow of the fluid injected into the crack, the pore fluid flow in the porous medium surrounding the crack, the deformation of the surrounding porous medium, fluid leakage from the crack to the surrounding porous medium, heat transfer between the crack and porous medium, and hydraulic fracture propagation. The interactions between such phenomena are reflected by appearing the main variable of a differential equation in another differential equation; as a result, the governing differential equations have common variables. This coupling is so strong that the equations form a system of nonlinear differential equations, which should be solved in a fully coupled form in order to completely model the complicated process of hydraulic fracturing. The fluid flow within the crack was modeled using Cubic law. The intrinsic permeability of the crack was modeled through the cubic law, and the flow within the crack was assumed to be Newtonian. It should be noted that fluid and heat leakage through the crack wall into the surrounding porous rock and the possible formation of a fluid lag zone were calculated in a fully coupled form without any simplifying assumptions.

The outline of this article is as follows: the governing equations together with initial and boundary conditions and constitutive relations are presented in section 2. In section 3, numerical simulation results and discussions are presented and finally some concluding remarks are given in section 4.

2. Formulation

In the process of non-isothermal propagation of hydraulic fracture in a saturated deformable porous media, considering the interaction of different physical mechanisms is essential. Considering solid phase displacements ($\mathbf{u}$), pore

fluid pressure (p_w) and temperature (T) as the main field variables, the set of partial differential equations governing this process can be summurized as follows [7], [28].

(1) The linear momentum balance equation for the whole mixture:

$$\boldsymbol{\sigma}_{ij,j} + \rho \mathbf{g}_i = 0 \tag{1}$$

(2) The continuity equation for the pore fluid flow through surrounding rock medium:

$$\begin{aligned} &(\frac{\alpha - n}{K_s} + \frac{n}{K_w})\dot{p}_w + \alpha \dot{\mathbf{u}}_{i,i} \\ &-[\beta_s(\alpha - n) + n\beta_w]\dot{T} \\ &+\frac{1}{\rho_w}\left[\rho_w \frac{\mathbf{k}_{ij}}{\mu_w}(-p_{w,j} + \rho_w \mathbf{g})\right]_{,i} = 0 \end{aligned} \tag{2}$$

(3) The continuity equation for the fluid flow within the fracture:

$$\begin{aligned} &\frac{1}{K_w}\frac{\partial p_w}{\partial t} + \frac{1}{w}\frac{\partial w}{\partial t} \\ &+\frac{1}{\rho_w}[\rho_w \bar{\mathbf{v}}_{wi'}]_{,i'} - \beta_w \dot{T} = 0 \end{aligned} \tag{3}$$

(4) The energy balance equation for surrounding rock medium:

$$\begin{aligned} &[(1-n)\rho_s C_s + n\rho_w C_w]\dot{T} \\ &+\rho_w C_w (\frac{\mathbf{k}_{ij}}{\mu_w}(-p_{w,j} + \rho_w \mathbf{g}))T_{,i} \\ &-(\boldsymbol{\lambda}_{ij} T_{,j})_{,i} - Q = 0 \end{aligned} \tag{4}$$

(5) The energy balance equation for the fracture medium (By neglecting the conductivity term and the source term):

$$\rho_w C_w \dot{T} + \rho_w C_w \dot{\mathbf{u}}_i^{ws} T_{,i} = 0 \tag{5}$$

Where $\boldsymbol{\sigma}_{ij}$ is the total stress tensor, and $\rho = (1-n)\rho_s + n\rho_w$ is the average density of the mixture. μ_w is the pore fluid dynamic viscosity and n denotes the porosity. $\mathbf{g}$ is the vector of gravity acceleration and α denotes Biot's parameter. ρ_s and ρ_w are the solid and pore fluid density and also K_s and K_w are solid grains and fluid phase bulk modulus, respectively. Moreover, β_s and β_w are thermal expansion coefficients of solid grains and pore fluid and C_s and C_w are their corresponding heat capacities. $\mathbf{k}_{ij}$ and $\boldsymbol{\lambda}_{ij}$ are the permeability and the conductivity tensors, respectively. w is the crack opening and $\bar{v}_{wi'}$ denotes the average velocity vector of the injected fluid within the fracture medium which is defined as:

$$\bar{\mathbf{v}}_{wi'} = k_{wd}(-p_{w,i'} + \rho_w \mathbf{g}_{i'}) \tag{6}$$

where $i' = 1,3$ which are the directions along the fracture length and height, respectively. k_{wd} is the fracture permeability that is defined through cubic law as follows:

$$k_{wd} = \frac{w^2}{12\mu_w f} \tag{7}$$

Where f denotes a coefficient between 1.04 and 1.65 which takes into account the crack wall roughness effects on the fracturing fluid flow [32]. The set of initial and boundary conditions (Fig. 1) can be described as follows:

(I) Initial conditions:

$$u_i = u_i^0, \quad p_w = p_w^0, \quad T = T^0 \text{ at } t = 0 \text{ on } \Omega \tag{7}$$

(II) Essential boundary conditions:

$$\begin{aligned} &u_i = \bar{u}_i \text{ on } \Gamma_u \ , \quad p_w = \bar{p}_w \text{ on } \Gamma_{p_w}, \\ &T = \bar{T} \text{ on } \Gamma_T \end{aligned} \tag{8}$$

(III) Natural boundary conditions:

$$\begin{aligned} &\sigma_{ij}.n_j = \bar{t}_i \quad \text{on} \quad \Gamma_\sigma \\ &\frac{k_{ij}}{\mu_w}(-p_{w,j} + \rho_w g_i).n_i = \bar{q}_w \quad \text{on} \quad \Gamma_{qw} \\ &\rho_w C_w \dot{u}_i^{ws} T.n_i - \lambda_{ij} T_{,j}.n_i = \bar{q}_T \quad \text{on} \quad \Gamma_{qT} \end{aligned} \tag{9}$$

(IV) Internal boundary conditions:

$$\begin{aligned} &\sigma_{ij}.n_{\Gamma_d} = t_d - p_w.n_{\Gamma_d} \quad \text{on} \quad \Gamma_d \\ &[\![\bar{V}_{wi}]\!].n_{\Gamma_d} = q_{Lw} \quad \text{on} \quad \Gamma_d \\ &\left[\!\!\left[\rho_w C_w \frac{k_{ij}}{\mu_w}(-P_{w,j} + \rho_w g)T - \lambda_{ij} T_{,j}\right]\!\!\right].n_{\Gamma_d} = q_{LT} \end{aligned} \tag{10}$$

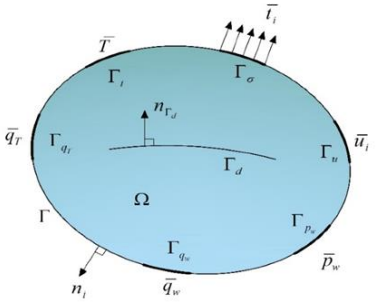

Fig. 1. Boundary conditions

In above equations, t_d denotes cohesive tractions along the discontinuity Γ_d at the fracture process zone which are related to the fracture opening through a proper constitutive law. In this study, a linear traction-separation law is used as shown in figure 2. This relation can be formulated as follows [31]:

$$\mathbf{t}_{coh} = \frac{-f_t^{\,2}}{2G_f}\omega + f_t \qquad (11)$$

Where f_t and G_f are the tensile strength and the fracture energy, respectively which are known as the model parameters for cohesive crack model.

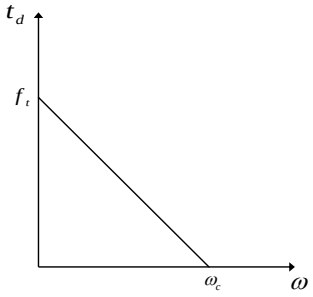

Fig. 2. Linear traction-separation law used in this study

In order to model weak and strong discontinuities, enrichment strategy is used in such a way that the desired properties can be reproduced properly. So, the Heavised enrichment function is used for strong discontinuities as follows:

$$H(\mathbf{x}) = \begin{cases} -1 & \text{if } \varphi(\mathbf{x}) < 0 \\ +1 & \text{if } \varphi(\mathbf{x}) \geq 0 \end{cases} \qquad (12)$$

Also, the Ridge function is used for simulation of weak discontinuities where the field variables are continuous but their first derivatives are discontinuous (Equation 13).

$$R(\mathbf{x}) = \sum_{I \in n^{enr}} N_I(\mathbf{x})|\varphi_I| - \left|\sum_{I \in n^{enr}} N_I(\mathbf{x})\varphi_I\right| \qquad (13)$$

It is worth to note that the function φ is known as the signed distance function, a kind of level set function for tracking the discontinuity surface [33], [34].

$$\varphi(\mathbf{x}) = \|\mathbf{x} - \mathbf{x}^*\| \operatorname{sign}(\mathbf{n}_{\Gamma_d} \cdot (\mathbf{x} - \mathbf{x}^*)) \qquad (14)$$

where $\|\mathbf{x} - \mathbf{x}^*\|$ is the distance between the discontinuity and point $\mathbf{x}$ and $\mathbf{n}_{\Gamma_d}$ is the unit normal vector to the interface at $\mathbf{x}^*$. N_I and n^{enr} in Equation (13) are the standard MLS shape function and the number of nodes whose supports intersect the line/surface of the discontinuity, respectively.

3. Numerical simulation results

In this section, the effects of temperature field on hydraulic fracture growth in an infinite saturated porous medium is investigated through numerical analysis. Heat flux in the fluid injection area can be caused by the injection of a hot fluid or chemical reactions upon acid injection in the crack opening. Therefore, heat flux can be applied to the computational domain in the fluid injection area. This assumption represents a fluid at a higher temperature compared to the medium temperature; i.e., a hot fluid is injected into the medium. The initial medium temperature and pore pressure are assumed to be zero and the in-situ stresses and gravity acceleration are disregarded. The fluid injection and heat flux duration was set to 10,000 s, at an injection rate of 3×10^{-6} m^2/s. Geometry and boundary conditions together with the inititial crack of 0.1 m long are depicted in figure 3.

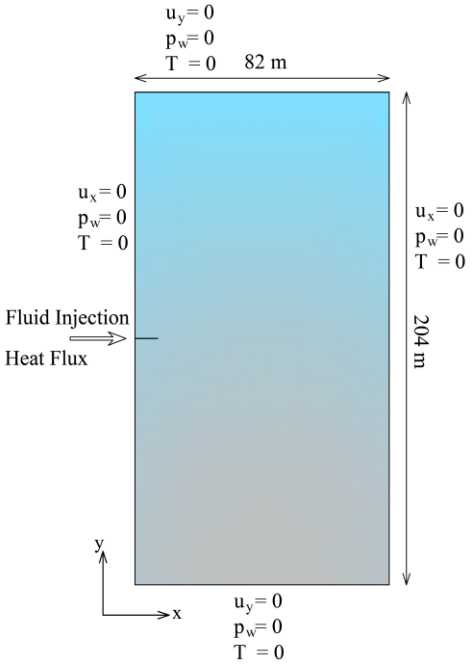

Fig. 3. Geometry and boundary conditions

Figure 4 illustrates the nodal arrangement of EFG model. The concentration of nodes near the injection area and along the fracture path is depicted in figure 5. The present study has explored the tempreture effects in two distint scenarios. First, the effects of a temperature rise were evaluated by increasing the thermal conductivity and applying heat flux in a larger area than the fluid injection area. Second, heat flux was applied in the fluid injection area under realistic conductivity coefficient condition, exploring the effects of convective heat transfer within the crack and studying the influence of conductivity on the outputs. Material properties are presented in Table 1.

Table 1. Material Properties

Property	Value	Unit
Intrinsic permeability	6×10^{-15}	m^2
Fracture energy	143	N/m
Tensile strength	0.45	MPa
Initial porosity	0.19	-
Fluid dynamic viscosity	0.001	Pa.s
Fluid phase density	1000	kg/m^3
Solid phase density	2000	kg/m^3
Elstic young modulus	15960	kPa
Poison's ratio	0.33	-
Biot coefficient	0.79	-
Fluid phase bulk modulus	3000	MPa
Solid phase bulk modulus	36000	MPa
Conductivity	1.0	J/sm°C
Fluid phase heat capacity	4184.0	J/kg°C
Soild phase heat capacity	837.0	J/kg°C
Fluid phase thermal expansion coefficient	6.3×10^{-6}	1/°C
Solid phase thermal expansion coefficient	9×10^{-7}	1/°C

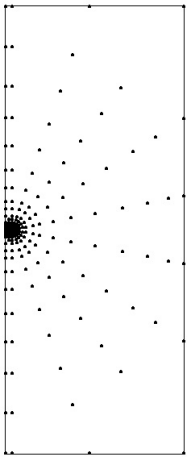

Fig. 4. Nodal arrangement for the computational domain

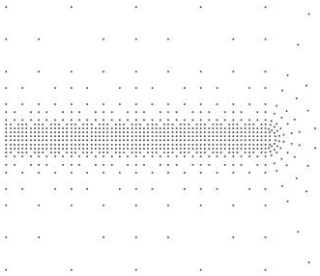

Fig. 5. Consentration of nodes near the injection area and along the fracture path

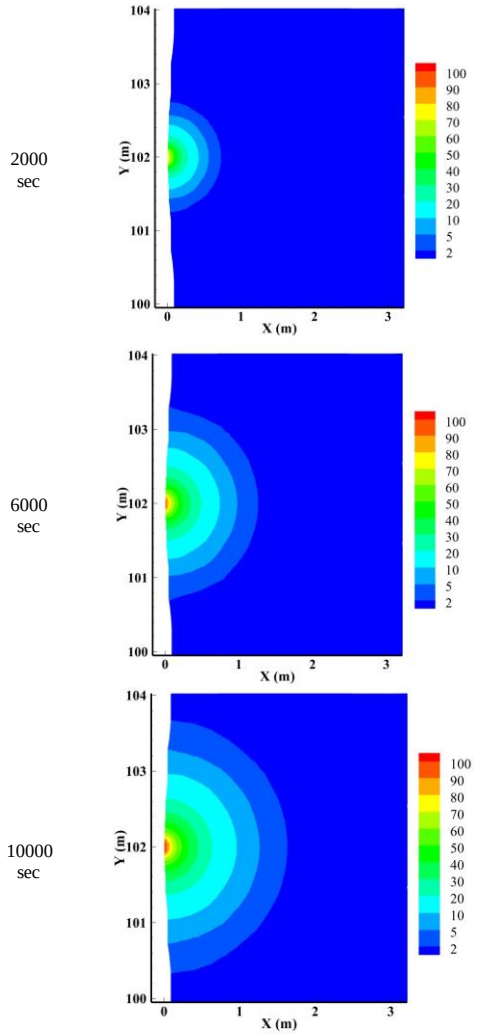

Fig. 6. Temperatre distribution near the injection area for scenario 1.

Scenario 1: To evaluate the effects of temperature on the crack length, crack mouth

opening displacement, and crack mouth pressure, the conductivity was unrealistically assumed to be 100 J/sm°C, with a heat flux of 5.5×104 W/m^2 applied to a length of 20 cm. Note that the fluid was injected at a length of 5 cm into the crack mouth. However, to capture the effects of the temperature during a period long enough to enable the heat to somewhat penetrate the medium, the heat flux was implemented along a longer length (20 cm).

Figure 6 depicts the temperature distribution for three injection durations. As can be seen, heat transfer occurred through the conduction mechanism around the crack and increased the surrounding rock temperature when relatively high heat flux was applied at an unrealistically high conductivity. Figures 7-9 illustrate the crack length, crack mouth opening displacement, and crack mouth pressure in the first scenario in comparison to the isothermal condition. Figure 7 shows that at the beginning of crack growth (until t=1000 s), the crack growth rate was larger than that in the isothermal condition due to the increased fluid pressure near the crack tip upon the temperature rise.

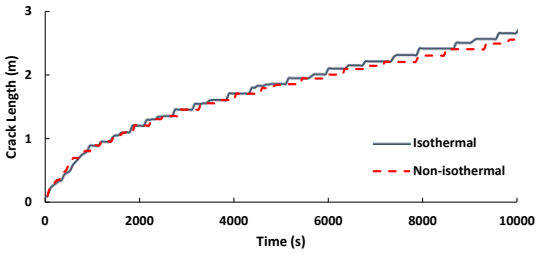

Fig. 7. Time variation of crack length for scenario 1.

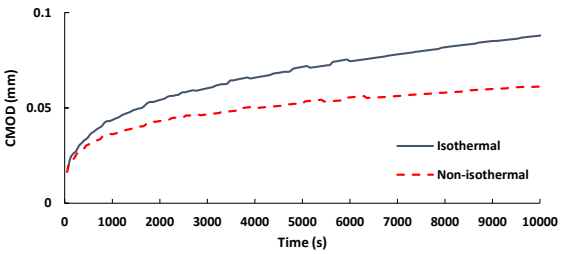

Fig. 8. Time variation of crack mouth opening displacement for scenario 1.

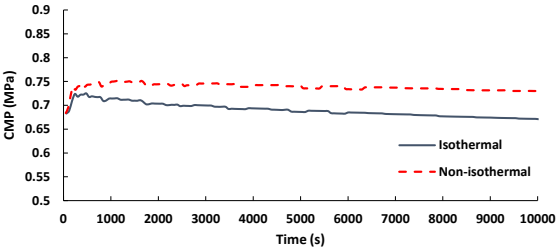

Fig. 9. Time variation of crack mouth pressure for scenario 1.

Afterwards, due to the conductive heat transfer in the surrounding porous medium and the subsequent rock expansion, the crack tends to close and the crack growth rate decreases compared to the isothermal condition. This is also reflected in the plot of crack mouth opening displacement over time (Figure 8). This figure shows that due to the temperature rise around the crack, rock expansion reduces the crack mouth opening displacement compared to the isothermal condition. Furthermore, the rise in temperature in the fluid injection area increased the crack mouth pressure relative to the isothermal condition (Figure 9).

Scenario 2: Now a heat flux of 2.4×10^4 W/m^2 is applied to the fluid injection area (5 cm). The thermal conductivity of the medium is assumed to be 1.0 J/sm°C, representing a more realistic coefficient. Figure 10 illustrates the temperature distribution for three injection durations.

As can be seen, under the realistic conductivity condition, heat transfer occurres only through the convection mechanism due to the fluid flow into the crack. Since the porous rock around the crack has a negligible conductivity coefficient, and convection would be low due to the low permeability of the medium, Therefore, heat transfer occurred only through convection within fracture medium. This demonstrates the validity of the formulation and the good performance of the numerical model in the coupling process.

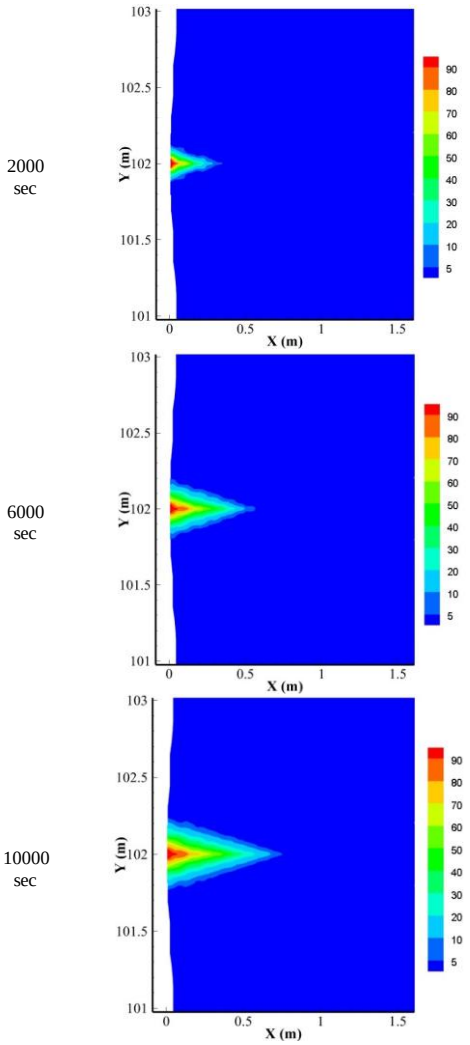

Fig. 10. Temperatre distribution near the injection area for scenario 2 ($\lambda = 1$ J/sm°C).

Then the conductivity of the medium was increased to 100 J/sm°C to investigate the effects of conduction heat transfer when heat flux is only applied to the fluid injection area. Figure 11 depicts the temperature distribution for this situation.

As can be seen, with increasing the conductivity coefficient, the applied heat distributes radially and diminishes in a short time, since the initial temperature of the domain is 0°C. Therefore, the medium temperature would not rise to a large extent, reaching nearly 15°C in the heat flux area. On the other hand, the heat deterioration rate was lower when the medium had a low conductivity coefficient, with the temperature rising to approximately 90°C, as shown in Figure 10.

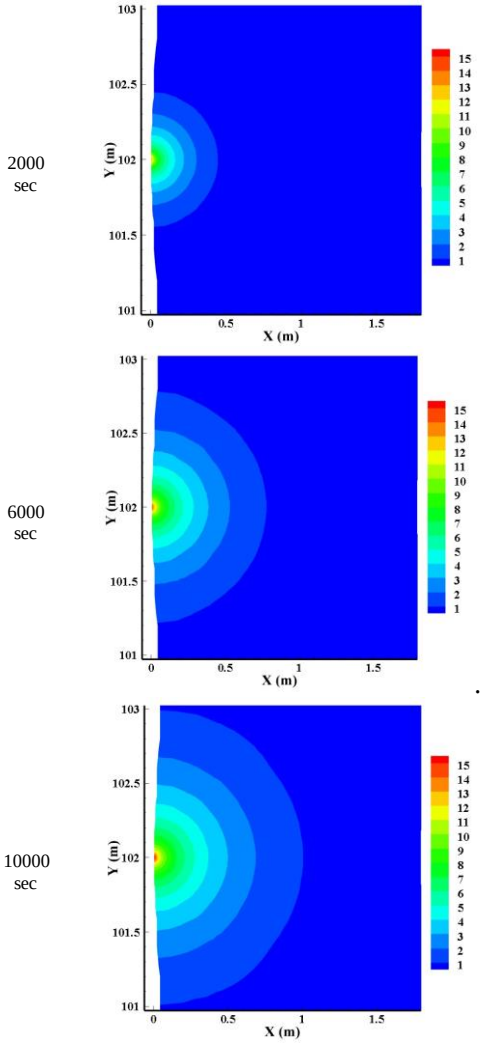

Fig. 11. Temperatre distribution near the injection area for scenario 2 ($\lambda = 100$ J/sm°C).

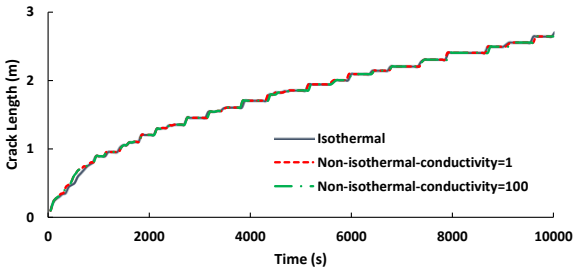

Fig. 12. Time variation of crack length for scenario 2.

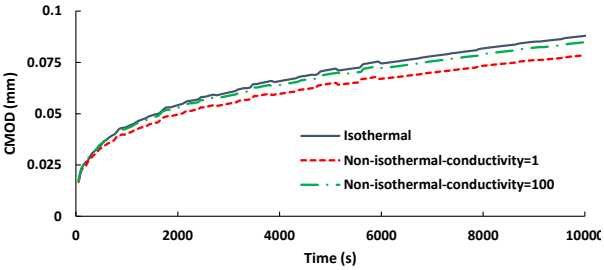

Fig. 13. Time variation of crack mouth opening displacement for scenario 2.

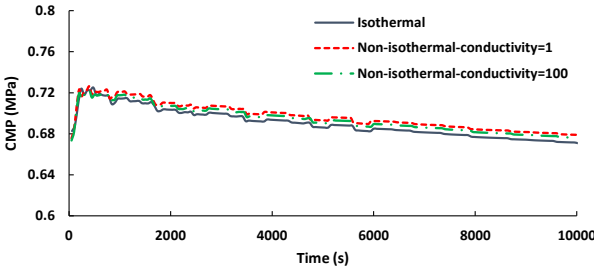

Fig. 14. Time variation of crack mouth pressure for scenario 2.

Figures 12-14 demonstrate the crack length, crack mouth opening displacement and crack mouth pressure for the second scenario at two different conductivity coefficients in comparison to the isothermal condition. According to Figure 12, at the beginning of crack growth (t=0 to 1000 s), the crack growth rate for both conductivity coefficients was found to be higher than that in the isothermal condition due to the increased fluid pressure near the crack tip arising from the temperature rise, same the first scenario. Later, the crack growth rate declined to almost the same level as that in the isothermal condition due to the increased distance between the crack tip and heated area and reduced temperature contribution to fluid pressure as a crack growth driver. The thermal expansion of the rock around the crack wall was another explanation, which induced a crack closing tendency and decelerated the crack growth. However, such a tendency was not large enough to reduce the crack growth rate below the isothermal growth rate.

According to Figure 13, the crack mouth opening displacement was smaller in the second scenario for both conductivity coefficients comparing to that in the isothermal condition; it was smaller at 1 J/sm°C than at 100 J/sm°C due to heat deterioration at higher conductivity coefficients. In other words, the expansion of the porous rock around the crack was lower at a conductivity of 100 J/sm°C than at 1 J/sm°C, leading to a lower crack closing tendency. According to Figure 14, the crack mouth pressure for both conductivities in the second scenario is higher than in the isothermal one. The pressure rise is expectedly higher at the conductivity of 1 J/sm°C than that at 100 J/sm°C since the temperature near the crack mouth is higher at the conductivity of 1 J/sm°C.

4. Conclusions

In this paper, the extended element free Galerkin method is utilized to simulate the fully coupled thermo-hydro-mechanical process of propagation of hydraulic fracture in saturated deformable porous media. To achieve this goal, the momentum balance equation of the whole mixture, continuity of fluid phase in host medium and fracture medium as well as energy balance equation in the host and fracture media are considered. Weak and strong discontinuities are modeled using enrichment strategy with proper enrichment functions and the cohesive crack model is employed to incorporate the non-linear behavior of near crack tip material. Convective heat transfer through the injected fluid flow into the fracture medium is explicitly modeled and the effects of conductive and convective heat transfer on hydraulic fracture parameters such as crack length, crack mouth opening displacement and crack mouth pressure are investigated. Numerical results show the good performance of the developed computer program in coupling the governing equations.

It can be concluded from the obtained results that the effects of heat flux at the injection area depend on factors such as the injection rate, the intensity of applied heat flux, the permeability of host rock, the permeability of fracture medium and the conductivity of porous media. This issue causes that the heat effects cannot be described as a constant effect.

4. References

[1] J. Geertsma and F. De Klerk, (1969) “Rapid Method of Predicting Width and Extent of Hydraulically Induced Fractures,” *J Pet. Technol.*, vol. 21, no. 12, pp. 1571–1581, doi: 10.2118/2458-pa.

[2] R. P. Nordgren, (1972) “Propagation of a Vertical Hydraulic Fracture,” *Soc. Pet. Eng. J.*, vol. 12, no. 04,

pp. 306–314, doi: 10.2118/3009-pa.

[3] J. Adachi, E. Siebrits, A. Peirce, and J. Desroches, (2007) "Computer simulation of hydraulic fractures," *Int. J. Rock Mech. Min. Sci.*, vol. 44, pp. 739–757, doi: 10.1016/j.ijmms.2006.11.006.

[4] K. Yamamoto, T. Shimamoto, and S. Sukemura, (2004) "Multiple fracture propagation model for a three-dimensional hydraulic fracturing simulator," *Int. J. Geomech.*, vol. 4, no. 1, pp. 46–57, doi: 10.1061/(ASCE)1532-3641(2004)4:1(46).

[5] B. Carter, J. Desroches, A. R. Ingraffea, and P. A. Wawrzynek, (2000) "Simulating fully 3D hydraulic fracturing," *Model. Geomech.*, Accessed: Dec. 26, 2014. [Online]. Available: http://www.cfg.cornell.edu/~bruce/papers/modeling_geomechanics_2000_carter_etal.pdf.

[6] M. C. Lobão, R. Eve, D. R. . Owen, and E. A. Souza Neto, (2010) "Modelling of hydro-fracture flow in porous media," *Eng. Comput.*, vol. 27, no. 1, pp. 129–154, doi: 10.1108/02644401011008568.

[7] T. Mohammadnejad and a. R. Khoei, (2013) "An extended finite element method for hydraulic fracture propagation in deformable porous media with the cohesive crack model," *Finite Elem. Anal. Des.*, vol. 73, pp. 77–95, Oct. doi: 10.1016/j.finel.2013.05.005.

[8] S. Salimzadeh and N. Khalili, (2015) "A three-phase XFEM model for hydraulic fracturing with cohesive crack propagation," *Comput. Geotech.*, vol. 69, pp. 82–92, doi: 10.1016/j.compgeo.2015.05.001.

[9] M. Vahab, S. Akhondzadeh, A. R. Khoei, and N. Khalili, (2018) "An X-FEM investigation of hydro-fracture evolution in naturally-layered domains," *Eng. Fract. Mech.*, vol. 191, no. February, pp. 187–204 , doi: 10.1016/j.engfracmech.2018.01.025.

[10] S. Samimi and A. Pak, (2016) "A fully coupled element-free Galerkin model for hydro-mechanical analysis of advancement of fluid-driven fractures in porous media," *Int. J. Numer. Anal. Methods Geomech.*, doi: 10.1002/nag.

[11] G. Tiankui, T. Songjun, L. Shun, L. Xiaoqiang, Z. Wei, and Q. Guanzheng, (2020) "Numerical simulation of hydraulic fracturing of hot dry rock under thermal stress," *Eng. Fract. Mech.*, p. 107350.

[12] W. Liu, Q. Zeng, and J. Yao, (2018) "Numerical simulation of elasto-plastic hydraulic fracture propagation in deep reservoir coupled with temperature field," *J. Pet. Sci. Eng.*, vol. 171, no. July, pp. 115–126.

[13] Z. Luo, L. Cheng, L. Zhao, and Y. Xie, (2022) "Numerical simulation and analysis of thermo-hydro-mechanical behaviors of hydraulic fracturing in naturally fractured formation using a THM-XFEM coupling model," *J. Nat. Gas Sci. Eng.*, vol. 103, no. August 2021, p. 104657.

[14] Z. Zhou, H. Mikada, J. Takekawa, and S. Xu, (2022) "Numerical Simulation of Hydraulic Fracturing in Enhanced Geothermal Systems Considering Thermal Stress Cracks," *Pure Appl. Geophys*, vol. 179, pp. 1775–1804.

[15] C. Yan, X. Xie, Y. Ren, W. Ke, and G. Wang, (2022) "A FDEM-based 2D coupled thermal-hydro-mechanical model for multiphysical simulation of rock fracturing," *Int. J. Rock Mech. Min. Sci.*, vol. 149, no. October 2021, p. 104964.

[16] S. Enayatpour, E. van Oort, and T. Patzek, (2019) "Thermal cooling to improve hydraulic fracturing efficiency and hydrocarbon production in shales," *J. Nat. Gas Sci. Eng.*, vol. 62, no. December 2018, pp. 184–201, doi: 10.1016/j.jngse.2018.12.008.

[17] M. S. Mortazavi, P. Pirmoradi, and A. R. Khoei, (2022) "Numerical simulation of cold and hot water injection into naturally fractured porous media using the extended – FEM and an equivalent continuum model," no. April, pp. 0–39, doi: 10.1002/nag.3314.

[18] S. M. S. Mortazavi and P. Pirmoradi, (2022) "Numerical simulation of cold and hot water injection into naturally fractured porous media using the extended – FEM and an equivalent continuum model," *Int. J. Numer. Anal. Methods Geomech.*, no. April, pp. 0–39.

[19] S. Salimzadeh, A. Paluszny, and R. W. Zimmerman, (2018) "Effect of Cold CO2 Injection on Fracture Apertures and Growth International Journal of Greenhouse Gas Control E ff ect of cold CO2 injection on fracture apertures and growth," *Int. J. Greenh. Gas Control*, vol. 74, no. April, pp. 130–141.

[20] H. Ghasemzadeh and S. A. Ghoreishian Amiri, (2013) "A hydro-mechanical elastoplastic model for unsaturated soils under isotropic loading conditions," *Comput. Geotech.*, vol. 51, pp. 91–100. http://dx.doi.org/10.1016/j.compgeo.2013.02.006.

[21] H. Ghasemzadeh, M. H. Sojoudi, S. A. Ghoreishian Amiri, and M. H. Karami, (2017) "Elastoplastic model for hydro-mechanical behavior of unsaturated soils," *Soils Found.*, vol. 57, no. 3, pp. 371–383, http://dx.doi.org/10.1016/j.sandf.2017.05.005.

[22] S. A. Sadmejad, H. Ghasemzadeh, S. A. Ghoreishian Amiri, and G. H. Montazeri, (2012) "A control volume based finite element method for simulating incompressible two-phase flow in heterogeneous porous media and its application to reservoir engineering," *Pet. Sci.*, vol. 9, no. 4, pp. 485–497 , doi: 10.1007/s12182-012-0233-6.

[23] S. A. Ghoreishian Amiri, S. A. Sadmejad, and H. Ghasemzadeh, (2017) "A hybrid numerical model for multiphase fluid flow in a deformable porous medium," *Appl. Math. Model.*, vol. 45, pp. 881–899, http://dx.doi.org/10.1016/j.apm.2017.01.042.

[24] M. A. Iranmanesh, A. Pak, and S. Samimi, (2018) "Non-isothermal simulation of the behavior of unsaturated soils using a novel EFG-based three dimensional model," *Comput. Geotech.*, vol. 99, pp. 93–103, doi: 10.1016/j.compgeo.2018.02.024.

[25] S. Samimi and A. Pak, (2012) "Three-dimensional simulation of fully coupled hydro-mechanical behavior of saturated porous media using Element Free Galerkin (EFG) method," *Comput. Geotech.*, vol. 46, pp. 75–83, doi: 10.1016/j.compgeo.2012.06.004.

[26] A. Tootoonchi, A. Khoshghalb, G. R. Liu, and N. Khalili, (2016) "A cell-based smoothed point interpolation method for flow-deformation analysis of saturated porous media," *Comput. Geotech.*, vol. 75, pp. 159–173 , doi: 10.1016/j.compgeo.2016.01.027.

[27] A. Khoshghalb and N. Khalili, (2010) "A stable meshfree method for fully coupled flow-deformation analysis of saturated porous media," *Comput. Geotech.*, vol. 37, no. 6, pp. 789–795, doi: 10.1016/j.compgeo.2010.06.005.

[28] R. W. Lewis and B. A. Schrefler, (1998) *The Finite Element Method in the Static and Dynamic Deformation and Consolidation of Porous Media*. Chichester: Wiley.

[29] G. R. Liu and Y. T. Gu, (2005) *An introduction to meshfree methods and their programming*. Dordrecht, The Netherlands: Springer.

[30] M. A. Iranmanesh and A. Pak, (2018) "Extrinsically enriched element free Galerkin method for heat and fluid flow in deformable porous media involving weak and strong discontinuities," *Comput. Geotech.*, vol. 103, no. July, pp. 179–192, doi: 10.1016/j.compgeo.2018.07.013.

[31] A. R. Khoei (2014), *Extended Finite Element Method*. Wiley.

[32] P. A. Witherspoon, J. S. Y. Wang, K. Iwai, and J. E. Gale, (1980) "Validity of cubic law for fluid flow in a deformable rock fracture," *Water Resour. Res.*, vol. 16, no. 6, pp. 1016–1024.

[33] G. Ventura, J. X. Xu, and T. Belytschko, (2002) "A vector level set method and new discontinuity approximations for crack growth by EFG," *Int. J. Numer. Methods Eng.*, vol. 54, no. 6, pp. 923–944, doi: 10.1002/nme.471.

[34] V. P. Nguyen, T. Rabczuk, S. Bordas, and M. Duflot, (2008) "Meshless methods: A review and computer implementation aspects," *Math. Comput. Simul.*, vol. 79, no. 3, pp. 763–813, doi: 10.1016/j.matcom.2008.01.003.